Interpreting Wind-Driven Southern Ocean Variability in a Stochastic Framework

Philip Sura [1] and Sarah T. Gille

Physical Oceanography Research Division,
Scripps Institution of Oceanography, La Jolla, California

August 8, 2002

Manuscript submitted to *JMR*

[1]Current affiliation: NOAA-CIRES, Climate Diagnostics Center
Corresponding author address: Philip Sura, NOAA-CIRES, Climate Diagnostics Center, R/CDC1, 325 Broadway, Boulder, CO 80305-3328, E-Mail: psura@cdc.noaa.gov

Abstract

A stochastic model is derived from wind stress and bottom pressure gauge data to examine the response of the Antarctic Circumpolar Current (ACC) transport to wind stress forcing. A general method is used to estimate the drift and diffusion coefficients of a continuous stationary Markovian system. As a first approximation, the response of the ACC to wind stress forcing can be described by a multivariate Ornstein-Uhlenbeck process: Gaussian red noise wind stress drives the evolution of the ACC transport, which is damped by a linear drag term. This stochastic model can serve as a null hypothesis for studies of wind driven ACC variability.

A more accurate stochastic description of the wind stress over the Southern Ocean requires a multiplicative noise component. The variability of the wind stress increases approximately linearly with increasing wind stress values. A multiplicative stochastic process generates a power-law distribution rather than a Gaussian distribution. A simple stochastic model shows that non-Gaussian forcing could have a significant impact on the velocity (or transport) probability density functions (PDFs) of the wind driven circulation. The net oceanic damping determines whether the distribution of the

oceanic flow is Gaussian (small damping) or resembles the distribution of the atmospheric forcing (large damping).

1 Introduction

Stochastic differential equations (SDEs) offer a useful formalism for describing the nonlinear dynamics of the atmosphere and ocean over a wide range of scales. The general idea of *stochastic climate models* was introduced by Hasselmann (1976) and is based on the Brownian motion analog: the observed red spectrum of oceanic fluctuations is a consequence of the amplification of low-frequency weather fluctuations. Stochastic climate models have been successful in describing ocean variability within a broad frequency band (see e.g., Imkeller and von Storch 2001).

Despite the fact that stochastic models have been successful in providing a null hypothesis for tropical and midlatitude oceanic variability, they have been used only rarely to interpret Southern Ocean variability. In one example, Weisse et al. (1999) studied the stochastically forced variability of the Antarctic Circumpolar Current (ACC) using a coarse resolution ocean general circulation model (OGCM). The goal of the present study is to investigate the stochastic properties of wind-driven ACC transport variability by means of an *empirical* stochastic model.

The mechanisms by which winds drive the ACC transport have been

the subject of extensive debate. The debate focuses on two viewpoints: as first suggested by Munk and Palmén (1951) the wind stress over the ACC might be balanced by topographic form stress. In contrast Stommel (1957) proposed that the ACC transport might be controlled by a Sverdrup balance. Rintoul et al. (2001) review recent work on the subject. The variations of ACC transport in relation to winds have been studied by a number of authors (e.g. Wearn and Baker 1980; Hughes et al. 2000). More recently, Gille et al. (2001) used bottom pressure records from Drake Passage to show that transport fluctuations appear to be driven by the wind stress rather than wind stress curl. Our analysis will revisit the BPR observations, by fitting stochastic models to the observed time series, using methods that have been tested for other components of the climate system (see e.g., von Storch and Zwiers 1999).

Most stochastically forced ocean models, whether simple or complex, introduce the atmospheric stochastic forcing as Gaussian white or red noise. Thus, in the models the strength of the atmospheric noise is held constant and does not depend on the state of the system. In nature, the strength of the noise may also depend on the state of the atmosphere itself, in which case the stochastic atmospheric forcing can be modeled as multiplicative noise.

Sura (2002) showed that a complete stochastic description of midlatitude sea surface wind observations requires a multiplicative (or state-dependent) white noise term. Physically, this indicates that the variability of midlatitude winds increases with increasing wind speed. In spite of the observational evidence for multiplicative noise, the impact of multiplicative stochastic forcing on ocean models has not been explored extensively.

In this study, an empirical stochastic model is derived from wind stress and bottom pressure gauge data to examine the response of the ACC transport to wind stress forcing. Section 2 introduces the method, in which the drift and diffusion coefficients of a continuous stationary Markovian system are estimated from the observations, using a relatively new technique. The data are described in section 3. Results presented in section 4 are based on a first approximation, which neglects multiplicative noise and holds the stochastic atmospheric forcing constant. In section 5 we explore the impact of more realistic multiplicative noise on the wind-driven ACC. Finally, section 6 provides a summary and a discussion.

2 Method

In this study a general method is used to estimate the drift and diffusion coefficients of the Fokker-Planck equation for a continuous stationary Markovian stochastic process (Siegert et al. 1998; Friedrich et al. 2000b,a; Gradišek et al. 2000). Markovian systems can be used to represent a wide class of physical processes. We consider the dynamics of a n-dimensional system governed by the following Itô-SDE:

$$\frac{d\vec{x}}{dt} = \vec{A}(\vec{x}) + \tilde{B}(\vec{x})\vec{\eta} \tag{1}$$

with the $n \times n$ matrix $\tilde{B}$. $\vec{A}$ represents the deterministic component of the state vector $\vec{x}$, and $\tilde{B}(\vec{x})\vec{\eta}$ is the stochastic component. Equations similar to (1) are commonly used in oceanography to represent oceanic float or drifter dispersion, where $\vec{x}$ represents the particle trajectory. In the case of floats A_i measures the background flow field and is zero in cases when there is no mean flow. The term $\tilde{B}$ is constant if the variance of the float or drifter displacements is invariant in space and time.

In the discussion that follows the noise components η_i are assumed to be independent Gaussian white noise processes:

$$\langle \eta_i(t) \rangle = 0, \qquad \langle \eta_i(t)\eta_i(t') \rangle = \delta(t - t') \,, \tag{2}$$

where $\langle ... \rangle$ denotes the averaging operator. This is consistent with the formalism of the Itô stochastic calculus, which appoximates discrete uncorrelated fluctuations as continuous white noise. Atmosphere and ocean processes are often represented by the Stratonovich calculus, in which rapidly fluctuating quantities with small but finite correlation times are parameterized as white noise. This paper makes use of the Itô interpretation, because this allows us to interpret the deterministic term $\vec{A}(\vec{x})$ as the effective drift and because it produces tractable equations that allow us to explore the role of stochastic processes in driving the ocean. For a detailed discussion of stochastic integration and the differences between Itô and Stratonovich SDEs see, for example, Horsthemke and Lefever (1984) or Gardiner (1985). In both calculi, the matrix $\tilde{B}(\vec{x})$ describes the variability of the state vector $\vec{x}$ as a function of the state itself. For example, a state-dependent noise term is required to model the gustiness of synoptic sea surface winds (Sura 2002).

The probability density function $p(\vec{x}, t)$ (PDF) of the Itô-SDE (1) is governed by the corresponding Fokker-Planck equation (e.g., Gardiner 1985; Horsthemke and Lefever 1984; Paul and Baschnagel 1999):

$$\frac{\partial p(\vec{x}, t)}{\partial t} = -\sum_i \frac{\partial}{\partial x_i} A_i p(\vec{x}, t) + \frac{1}{2} \sum_{i,j} \frac{\partial^2}{\partial x_i \partial x_j} (\tilde{B}\tilde{B}^T)_{ij} p(\vec{x}, t) \,. \tag{3}$$

The Fokker-Planck equation describes the conservation of the probability density $p(\vec{x}, t)$ of the system described by the SDE. The first term on the right describes the dynamics of the deterministic system and is called the deterministic drift. The second term causes the diffusion of the system. In the classic examples of Brownian motion or float dispersion, with $A_i = 0$ and constant $\tilde{B}$, the PDF $p(\vec{x}, t)$ evolves in time. In the observations that we will discuss, the presence of non-zero A_i makes the PDF stationary in time.

Equations for the second moments of $\vec{x}$, representing variance or Reynolds stresses for example, can be obtained by multiplying the Fokker-Planck equation (3) by $x_p x_q$ and integrating over the domain of the system. That is,

$$\frac{\partial \langle x_p x_q \rangle}{\partial t} = \langle A_p x_q \rangle + \langle A_q x_p \rangle + \sum_i \langle B_{pi} B_{qi} \rangle \,. \tag{4}$$

This equation is known as the generalized fluctuation-dissipation relation (GFDR) of the system. The GFDR relates the variance of the stochastic fluctuations to the magnitude of the dissipation.

The deterministic and stochastic parts of (3) can be determined directly from data by using their statistical definitions:

$$\vec{A}(\vec{x}) = \lim_{\Delta t \to 0} \frac{1}{\Delta t} \langle \vec{X}(t + \Delta t) - \vec{x} \rangle |_{\vec{X}(t) = \vec{x}} \tag{5}$$

$$\tilde{B}(\vec{x}) \tilde{B}^T(\vec{x}) = \lim_{\Delta t \to 0} \frac{1}{\Delta t} \langle (\vec{X}(t + \Delta t) - \vec{x})(\vec{X}(t + \Delta t) - \vec{x})^T \rangle |_{\vec{X}(t) = \vec{x}} \tag{6}$$

where $\vec{X}(t+\Delta t)$ is a solution (a single stochastic realization) of the SDE (1) with the initial condition $\vec{X}(t) = \vec{x}$ at time t. The data define a state space representing every observed value of $\vec{x}$. Deterministic and stochastic parts of the underlying dynamics can be estimated at every point $\vec{x}$ at which there are sufficient observations. Note that the theoretical limit $\Delta t \to 0$ must be replaced by a finite-difference approximation. (See Sura (2002) or Sura and Barsugli (2002) for the univariate error estimation in the case of a finite time increment Δt.)

Analytical functions can be fitted to the empirical estimates of $\vec{A}(\vec{x})$ and $\tilde{B}(\vec{x})\tilde{B}^T(\vec{x})$ to derive model equations describing the system under consideration. In order to verify the results, the estimated functions $\vec{A}(\vec{x})$ and $\tilde{B}(\vec{x})\tilde{B}^T(\vec{x})$ can be inserted into the Fokker-Planck equation (3), and the resulting PDF can be compared with the PDF obtained directly from the data.

Note that $\tilde{B}(\vec{x})\tilde{B}^T(\vec{x})$ rather than $\tilde{B}(\vec{x})$ is estimated from data. In general it is impossible to find a unique expression for $\tilde{B}(\vec{x})$ in the multivariate case, because $\tilde{B}(\vec{x})$ is not guaranteed to be invertible. However, in the univariate case $B(x) = \sqrt{B(x)^2}$. The sign of the square root is arbitrary because $B(x)$ is

multiplied by Gaussian white noise with zero mean. Thus, in the univariate case even the SDE (1) can be used to test the estimates of $A(x)$ and $B(x)$ by simply comparing the properties (e.g., moments, spectra etc.) of the original time series with the properties of the time series obtained by integrating (1).

The technique described here has been successfully applied to a wide class of problems. For example, Friedrich and Peinke (1997a), Friedrich and Peinke (1997b), and Renner et al. (2001) describe statistical properties of a turbulent cascade. Friedrich et al. (2000a) quantify deterministic and stochastic influences on the foreign exchange market. Geophysical examples are provided by Ditlevsen (1999), who fitted a Fokker-Planck equation to ice core data, and Egger (2001), Egger and Jonsson (2002), and Sura (2002), who stochastically describe meteorological data sets.

3 Data

Here we examine the response of the ACC transport to wind stress forcing by analyzing bottom pressure and wind reanalysis products within a stochastic framework. The data used in this study have been used previously to study ACC transport variability in relation to wind forcing (e.g. Gille 1999;

Gille et al. 2001). Bottom pressure gauges were deployed on either side of Drake Passage from November 1992 through November 1997 by Proudman Oceanographic Laboratory. As in previous studies, here we infer geostrophic transport fluctuations from the time-varying pressure difference across Drake Passage, shown in Figure 1. The original data were sampled at 15 min or hourly interval, filtered to remove the semidiurnal/diurnal tidal signal, and subsampled at 12 hour intervals. Gaps in the pressure difference data are filled by linear interpolation.

Winds are represented by European Centre for Medium-Range Weather Forecasts (ECMWF) reanalysis for the 5-year period between 1992 and 1997. The wind stress and the wind stress curl are averaged zonally over the full Southern Ocean and meridionally between 50°S and 60°S, corresponding to the approximate latitude band of the ACC at Drake Passage. Figure 1 shows the time series for wind stress and wind-stress curl. Note that averaged zonal wind stress is very rarely negative. In the following all time series are normalized to have zero mean and unit standard deviation. For a more detailed description and a coherence analysis of the data see Gille et al. (2001).

4 Empirical Stochastic Models of the ACC

The mechanisms controlling ocean response to wind forcing depend on both the wind and the ocean transport. For this two component system, the governing SDE is

$$\begin{aligned} \frac{dx_1}{dt} &= A_1(x_1, x_2) + \sigma_1 \eta_1 \\ \frac{dx_2}{dt} &= A_2(x_1, x_2) + \sigma_2 \eta_2 \end{aligned} \tag{7}$$

where x_1 represents wind stress in section 4.1, and wind stress curl in section 4.2, and x_2 is the pressure difference across Drake Passage. Our findings show that the oceanic transport does not affect the atmospheric wind field, so that $A_1(x_1, x_2) = A_1(x_1)$. Note that (7) and all subsequent equations are dimensionless because the data are normalized.

In our analysis, we make two assumptions. First, the atmospheric wind field is expected to be unaffected by oceanic noise, and vice versa. Based on this assumption, the governing equations are simplified by assuming that the matrix $\tilde{B}$ is diagonal with elements σ_1 and σ_2. Second, in this section the noise term is not treated as a function of the state of the system. This means that the matrix $\tilde{B}$ is assumed to be constant. The first assumption is physically reasonable, but the second assumption is an approximation which

is not generally valid. As Sura (2002) has shown, a proper stochastic description of synoptic midlatitude sea surface winds requires a multiplicative noise component. The advantage of representing the wind stress as a red-noise process with constant $\tilde{B}$ is that the resulting SDE (7) can then be handled analytically. The impact of a more realistic stochastic wind stress forcing on the wind driven ACC variability will be discussed in section 5.

To evaluate A_1, A_2, σ_1, and σ_2 numerically, using the two-dimensional versions of Eqs. (5) and (6), the interval spanned by the data is divided into 50×50 equal bins. (Sensitivity experiments with different numbers of bins were performed as well, but the general results discussed below did not change). Because in this section the stochastic terms are treated as constants, the results of Eq. (6) are averaged to obtain σ_1 and σ_2. Then, σ_1 and σ_2 are cross-checked by comparing the direct numerical estimates with the results obtained from the GFDR. The smallest possible discrete time step of half a day is used for Δt in the finite-difference approximation. Since the method assumes that the data are Markovian, we verify that the method yields stable and physically reasonable results for different numbers of bins and, more importantly, for different discrete time steps Δt. A lack of convergence could indicate that the process had non-Markovian properties; however, in this

study the results converge stably as Δt decreases, and the results are therefore consistent with the assumption that the data are Markovian.

The disadvantage of the method used here is that for short time series such as these, the standard error of the mean in (5) and (6) can be large. This is particularly true in the multivariate case. Nevertheless, even for relatively large uncertainties the results can be tested by comparing the properties of the original data with the properties of the time series obtained by integrating (7).

4.1 Bottom pressure versus wind stress

The deterministic part of the wind stress time series, $A_1(x_1)$, is shown in Fig. 2. The term $A_1(x_1)$ decreases with increasing values of x_1, meaning that it acts to damp the wind stress, and can be approximated by a linear function. This means that as a first approximation the wind stress can be represented as a univariate Ornstein-Uhlenbeck process. The decorrelation time scale is the inverse of the (dimensional) damping coefficient, which therefore is the typical damping time scale of the system under consideration. In these data the atmospheric decorrelation time scale appears to be about 10 days for the

zonally and meridionally averaged wind stress. The local decorrelation time scale is much shorter, about 1 day (Sura 2002).

The estimated function $A_2(x_1, x_2)$ is shown in Fig. 3. Note that in this two-dimensional case the errors are not shown. The uncertainties are relatively large: the standard error is about 0.1 - 0.2 for center points, and up to 0.3 for a few border points. Because of the large uncertainty, we performed tests in order to see whether the same results could be found in random, uncorrelated time series. Our tests showed that the qualitative structure of $A_2(x_1, x_2)$ (discussed below) could not be reproduced by such a random process. As a second test of the robustness of the results, we compared the original data with the time series obtained by integrating the SDE. This analysis concentrates on the qualitative aspects of the results which are robust and physically consistent. The deterministic part of the oceanic time series consists of a forcing and damping term. The forcing can be identified by the overall positive gradient of $A_2(x_1, x_2)$ in the direction of x_1, whereas the damping is due to the dominant negative gradient in the direction of x_2. The function $A_2(x_1, x_2)$ can be approximated by a planar fit.

Assuming a linear fit to the entire deterministic drift the corresponding

two-dimensional SDE is

$$\begin{aligned} \frac{dx_1}{dt} &= -ax_1 + \sigma_1\eta_1 \\ \frac{dx_2}{dt} &= -bx_2 + cx_1 + \sigma_2\eta_2 \quad . \end{aligned} \tag{8}$$

See the appendix for more details on multivariate Ornstein-Uhlenbeck processes such as this. The covariance matrix of (8) can be evaluated to calculate the spectra and cross-spectra by Fourier transforming the appropriate elements of the covariance matrix: see (A.6), (A.7), and (A.8). Using the GFDR (or the covariance matrix) and assuming stationary statistics, the first moments of the variables x_1 and x_2 can be obtained:

$$\begin{aligned} \langle x_1^2 \rangle &= \frac{\sigma_1^2}{2a} \\ \langle x_2^2 \rangle &= \frac{c}{b}\langle x_1 x_2 \rangle + \frac{\sigma_2^2}{2b} = \frac{c^2\,\sigma_1^2}{2ab(a+b)} + \frac{\sigma_2^2}{2b} \\ \langle x_1 x_2 \rangle &= \frac{c}{(a+b)}\langle x_1^2 \rangle = \frac{c\,\sigma_1^2}{2a(a+b)} \quad . \end{aligned} \tag{9}$$

The estimated parameters are summarized in Table. 1. These parameters and the equation for $\langle x_2^2 \rangle$ together indicate that about 30% of ACC variability is driven by the wind stress, whereas 70% is due to processes that are not included in our simple model, and are, therefore, parameterized by noise.

The parameters derived in (8) can be used to estimate the spectral coherence of the wind with ACC transport and the phase difference between the

two systems. Fig. 4 shows the results of this estimation. The negative values of the phase ϕ indicate that the wind stress leads the oceanic transport. Fig. 4 indicates that for time periods longer than about 100 days wind stress and transport have constant and relatively high coherence. The coherence rapidly decrease for periods below 100 days. In the high coherence regime the oceanic transport lags the atmospheric forcing by about 60° for periods of 100 days; the phase lag becomes zero for very low frequencies (or long periods). Deterministic models suggest that at high frequencies wind should accelerate the ocean velocity, so that ACC transport lags wind by 90°. However, because of the low coherence at high frequencies, phase lags near 90° are not observed within the stochastic framework.

We test the estimates of $A_1(x_1)$, $A_2(x_1, x_2)$, σ_1, and σ_2 obtained by integrating (8) against the original bottom pressure difference time series. This is done by comparing the spectra and histograms of the original data with the corresponding "artificial" data (see Fig. 5). SDE (8) is solved by the stochastic Euler scheme (see e.g., Kloeden and Platen 1992).

Fig. 5a shows the spectra of the original data and of the artifical data simulated by the stochastic model. Both indicate red noise behavior (with

slopes $\propto \omega^{-2}$), as expected from the stochastic climate scenario proposed by Hasselmann (1976). A striking difference can be seen in the spectra at very high frequencies. The stochastic model does not reproduce the steep dip of the original data at frequencies of about 0.3 cycles per 0.25 days. The low-pass filter used to remove tidal signals has removed high-frequency energy from the observations, but that effect is not reproduced by the stochastic model. It is known that Markov models are not capable of reproducing steep spectral dips at very high frequencies (DelSole 2000). Because by construction both the original and the artifical data have the same overall variance, the spectra differ for frequencies below about 0.3 cycles per 0.25 days, even if the slopes are identical. Fig. 5b shows that the original data obey the Gaussian distribution of the stochastic model. Both histograms are identical on the basis of the Kolmogorov-Smirnov test.

To summarize, the linear stochastic model reproduces the general spectral characteristics and the PDF of the original data. Furthermore, the stochastic method yields results that are qualitatively similar to those obtained by Gille et al. (2001) using coherence analysis. The linear stochastic model does not reproduce a constant phase lag of about 20° observed by Gille et al. (2001). This may occur because the constant phase lag observed in the data

is a nonlinear effect, which is neglected within the linear approximation of the deterministic term $A_2(x_1, x_2)$. Nevertheless, the linear stochastic model reproduces the observational result indicating that the coherence increases with increasing period.

4.2 Bottom pressure versus wind stress curl

In this section, we explore the relation of ACC transport variability to wind stress curl. In this case, the term $A_1(x_1)$ acts to damp the wind stress curl nearly linearly (not shown), with a damping time scale of about 5 days. The estimated function $A_2(x_1, x_2)$ (not shown) is qualitatively similar to the results based on wind stress shown in Fig. 3: the deterministic part of the oceanic time series consists of a forcing and damping term, and the function $A_2(x_1, x_2)$ can again be approximated by a planar fit. See Table 1 for the estimated parameters and Fig. 4 for the coherence spectrum and the corresponding phase shift of (9). These results indicate that about 10% of ACC variability is driven by the wind stress curl, whereas 90% is due to the noise.

Fig. 4 shows that the overall coherence between wind stress curl and

transport is lower than in the case of pure wind stress. Nevertheless, there is still a regime with constant and relatively high coherence for periods longer than about 50 days; below 50 days the coherence rapidly decreases. In the high coherence regime, the oceanic transport lags the atmospheric forcing by about 85° for periods of 50 days, and rises to 0° for longer periods.

The coherence spectrum obtained using stochastic techniques are consistent with Gille et al.'s (2001) observations showing that phase lags between wind stress curl and bottom pressure were between 0° and 90°. In addition, both the observed observations and the time series simulated by the linear stochastic model indicate low coherence between wind forcing and ocean transport, and the linear stochastic model reproduces the increasing coherence with increasing period that is seen in the observations. Because of the low overall coherence between wind stress curl and transport, transport fluctuations appear more likely to be driven by wind stress than wind stress curl.

4.3 The stochastic Wearn-Baker model

As a first approximation the response of the ACC to wind stress forcing can be understand in terms of the stochastic version of the simple model introduced by Wearn and Baker (1980). In their model the time evolution of the transport $U(t)$ is simply due to the wind stress $\tau_x(t)$ and a linear drag term scaled by b:

$$\frac{\partial U}{\partial t} = -bU + \tau_x(t) \quad . \tag{10}$$

Wearn and Baker (1980) derived an analytic solution for a deterministic sinusoidal forcing $\tau_x(t) = \tau_0 \exp(i\omega t)$. The solution of the "deterministic Wearn-Baker model" is

$$U(t) = \frac{\tau_0}{\sqrt{b^2 + \omega^2}} \exp(i\omega t - \phi), \tag{11}$$

where $\phi = \arctan(-\omega/b)$. Therefore, in the sinusoidally forced deterministic case the variance of the transport becomes

$$< U^2(t) >= \frac{\pi\, \tau_0^2}{(b^2 + \omega^2)} \quad . \tag{12}$$

The previous results showed that the ocean transport appears to be driven by a stochastic red noise wind stress forcing (neglecting the multiplicative character of the wind stress forcing to be discussed in section 5). The gov-

erning SDE for the wind stress is

$$\frac{d\tau_x}{dt} = -a\tau_x + \eta \tag{13}$$

with the Gaussian white noise η. The solution for the wind stress is

$$\tau_x(t) = \exp(-at) \int_0^t \exp(as) dW(s) \quad . \tag{14}$$

where dW is the incremental change of the Wiener process W. Using this red noise process to force the model (11) the variance of the transport in the "stochastic Wearn-Baker model" becomes

$$< U^2(t) >= \frac{< \tau_x^2 >}{(b^2 + ab)} \quad . \tag{15}$$

Thus the variance in (15) resembles the variance from the the Wearn-Baker model, (12), with the deterministic frequency term, ω^2, replaced by the product of the inverse atmospheric and oceanic decorrelation time scales ab.

5 The Role of Multiplicative Noise

5.1 Multiplicative noise in stochastic forcing

This section examines how a multiplicative noise alters the linear stochastic models derived in section 4. The one-dimensional SDE equation to describe

the wind stress data is now written as

$$\frac{dx_1}{dt} = A_1(x_1) + B_1(x_1)\eta_1 \tag{16}$$

where x_1 is the wind stress, $A(x_1)$ is the deterministic, and $B_1(x_1)\eta_1$ the stochastic part. As shown in section 4.1 and in Fig. 2, the deterministic term $A_1(x_1)$ acts to damp the wind stress and can be approximated by a linear function. In this section, the function $B_1(x_1)$ is no longer constant, but depends on the state of the system, as shown in Fig. 6. The amplitude of the white noise forcing increases approximately linearly with increasing wind stress values. Therefore, the behavior of the multiplicative noise in the averaged wind stress data is qualitatively consistent with the results obtained by Sura (2002), who used local winds to show that the variability of midlatitude winds increases with increasing wind speed. Thus, a more complete stochastic description of the wind stress data would require a state dependent white noise forcing term. As a result of this state-dependent forcing, an Ornstein-Uhlenbeck process is not sufficient to describe the wind stress data within a stochastic framework.

5.2 Stochastic Wearn-Baker driven by a multiplicative wind stress forcing

Most stochastically forced ocean models implement the atmospheric stochastic forcing as *Gaussian* white or red noise. In particular, Gaussian red noise is modeled by a univariate Ornstein-Uhlenbeck process (13). There, the strength of the atmospheric noise is held constant and does not depend on the state of the system. Nevertheless, as shown in the previous section, a more accurate stochastic description of the wind stress data requires a state dependent white noise forcing term. It is well known that a multiplicative stochastic process generates a power-law distribution in contrast with the Gaussian distribution of an Ornstein-Uhlenbeck process (e.g., Schenzle and Brand 1979; Succi and Iacono 1986; Sakaguchi 2001). In this section the stochastic Wearn-Baker model serves as a toy-model to illustrate the effect of a more realistic *non-Gaussian* wind forcing on the variability of the oceanic circulation. We will consider the following stochastic model:

$$\begin{aligned} \frac{d\tau}{dt} &= -a\tau + \sqrt{2M}\,|\tau|\eta_M + \sqrt{2D}\,\eta_D \\ \frac{dU}{dt} &= -bU + \tau \end{aligned} \tag{17}$$

with Gaussian white noise satisfying

$$\langle \eta_M(t)\eta_M(t')\rangle = \delta(t-t') \ , \ \langle \eta_D(t)\eta_D(t')\rangle = \delta(t-t')\,. \tag{18}$$

M and D are constants governing the strength of the additive and multiplicative noise terms. The first equation models the wind stress τ by a simple linear damping term, and a combination of a state dependent and constant noise terms. The ocean transport U is driven solely by the stochastic wind stress and retarded by a linear damping term.

The stationary PDF of the wind stress τ has the form (Sakaguchi 2001):

$$p(\tau) = \Theta(D + M\tau^2)^{-\Pi} \tag{19}$$

with $\Pi = (a+2M)/2M$. The normalization constant Θ is given by:

$$\Theta = \frac{M^{1/2}D^{\Pi-1/2}}{\beta(1/2, \Pi-1/2)} = \frac{M^{1/2}D^{\Pi-1/2}\Gamma(\Pi)}{\Gamma(1/2)\Gamma(\Pi-1/2)} \tag{20}$$

where $\beta(x,y)$ is the beta function, and $\Gamma(x)$ is the gamma function: $\beta(x,y) = \Gamma(x)\Gamma(y)/\Gamma(x+y)$. The variance of the wind stress τ can be calculated as

$$\int_{-\infty}^{\infty} \tau^2 p \, d\tau = <\tau^2> = \frac{D}{a-M}\,. \tag{21}$$

Fig. 7 shows distributions $p(\tau)$ as defined by Eqs. (19) and (20) for $a = 1$, $D = 1$, with different strengths of the multiplicative noise M. For $M \to 0$,

the distribution becomes Gaussian with the variance D/a. The multiplicative noise causes the tails of the distribution to be heavier than they would be in the corresponding Gaussian distribution.

For the limits of very large and small b the probability distribution of U can be determined analytically. For large b the time derivative of U can be neglected:

$$U = \frac{\tau}{b} \tag{22}$$

Therefore,

$$\frac{dU}{dt} = \frac{1}{b}\frac{d\tau}{dt} = -aU + \sqrt{2M}\,|U|\eta_M + \sqrt{2D}\,\frac{\eta_D}{b}\,. \tag{23}$$

Thus, in (19) and (20) we substitute D/b^2 in place of D to obtain the distribution of U:

$$p(U) = \Upsilon\left(\frac{D}{b^2} + M\,U^2\right)^{-\Pi} \tag{24}$$

with the normalization constant Υ given by

$$\Upsilon = \frac{M^{1/2}(D/b^2)^{\Pi-1/2}}{\beta(1/2, \Pi - 1/2)} \tag{25}$$

Thus, when friction b is small, ocean transport is expected to have a power-law distribution.

For small b, $dU/dt = \tau$ so $U = \sum_j \tau_j \Delta t$, and the central limit theorem applies. That means, the distribution $p(U)$ becomes Gaussian with the vari-

ance $< U^2 >$, which is determined by the stationary version of the GFDR (4):

$$< U^2 >= \frac{< \tau^2 >}{b(a+b)} = \frac{D}{(a-M)b(a+b)} \,. \tag{26}$$

For intermediate b the distribution $p(U)$ will be somewhere in between the Gaussian and the power-law. More precisely, the damping determines whether the PDF of the wind-driven oceanic flow is Gaussian (small damping) or resembles the distribution of the atmospheric forcing (large damping). This is, of course, a very crude model of the wind-driven ocean circulation. Nevertheless, it shows that oceanic velocity PDFs can exhibit non-Gaussian behavior, as long as the atmospheric forcing is non-Gaussian as well. Since wind pdfs have been observed to be non-Gaussian, this may heuristically explain why velocity PDFs obtained from ocean observations show a non-Gaussian behavior in certain regions (Llewellyn Smith and Gille 1998; Gille and Llewellyn Smith 2000; Bracco et al. 2000). Why, then, do the ACC transport fluctuations shown in Fig. 5b appear Gaussian? First, in this region only 30% of ACC variability is driven by the wind stress, whereas 70% is due to processes that are not included in our model. Second, the time series is too short to detect non-Gaussian behavior in the tails of the distribution.

6 Summary and Discussion

An empirical stochastic model has been derived from wind stress and bottom pressure gauge data in order to examine the response of the Antarctic Circumpolar Current (ACC) transport to wind stress forcing. A general method is used to estimate the drift and diffusion coefficients of a continuous stationary Markovian system. As a first approximation, the response of the ACC to wind stress forcing can be described by a multivariate Ornstein-Uhlenbeck process: Gaussian red noise wind stress drives the evolution of the ACC transport that is damped by a linear drag term. The spectrum of the ACC transport fluctuations is red, as expected from the stochastic climate scenario proposed by Hasselmann (1976). The empirical model shows nearly the same behavior as revealed by coherence analysis of the same data set (Gille et al. 2001). The linear stochastic model does not reproduce a constant phase lag of about 20° between wind stress and ACC transport as observed by Gille et al. (2001), but rather shows the classical frequency dependent phase (Wearn and Baker 1980). The constant phase lag observed in the data is believed to be due to nonlinear effects that are not captured by the linear approximation. Despite this deficiency, the stochastic model can

serve as a null hypothesis for studies of wind-driven ACC variability. That is, the stochastic Wearn-Baker model is actually the simplest null hypothesis the describe wind-driven ACC variability.

In light of Hasselmann's theory this is actually not a very surprising results. It rather emphasizes the importance of *stochastic climate models* once again. Much more important is the fact that a more accurate stochastic description of the wind stress data over the Southern Ocean requires a multiplicative noise component. The variability of the wind stress increases with increasing wind stress values. This behavior has been discussed in more detail by Sura (2002). Most importantly, a multiplicative stochastic process generates a power-law distribution rather than a Gaussian distribution.

Using a simple stochastic model, it is shown that non-Gaussian forcing may have a significant impact on the velocity (or transport) PDFs of the wind driven ocean circulation. If the oceanic damping is small, the ocean has a very long memory, and oceanic velocities will represent a summation of many independent wind forcings. Then, as a result of the central limit theorem, the ocean velocities should have a Gaussian distribution, provided that the wind forcing PDF has finite variance. On the other hand, if the oceanic damping

is large, the ocean has little memory, and ocean velocities will reflect wind velocities. In this case the wind driven velocities will have distributions like the wind forcing distributions. The real ocean must lie somewhere in between these extremes, sometimes showing Gaussian pdfs and sometimes pdfs that resemble those of the wind forcing. The implications of these results are clear: in order to interpret observed oceanic velocity PDFs in a physical meaningful sense, the impact of a non-Gaussian wind forcing on the ocean circulation will need to be explored in the future using more complicated models.

Acknowledgments. Bottom pressure data for this study are archived by the Proudman Oceanographic Laboratory at www.pol.ac.uk/psmslh/gloup/gloup.html. This work was funded through the NASA Ocean Vector Wind Science Team, JPL Contract number 1222984.

Appendix

Multivariate Ornstein-Uhlenbeck process

In this appendix the properties of the multivariate Ornstein-Uhlenbeck process are discussed briefly. For a more comprehensive discussion see e.g. Gardiner (1985), Horsthemke and Lefever (1984), or Kloeden and Platen (1992).

The multivariate Ornstein-Uhlenbeck process is defined by the Itô SDE

$$\frac{d\vec{x}}{dt} = \tilde{A}\vec{x} + \tilde{B}\vec{\eta}, \tag{A.1}$$

where $\tilde{A}$ and $\tilde{B}$ are constant $n \times n$ matrices. The stochastic components η_i are assumed to be independent Gaussian white noise processes:

$$\langle \eta_i(t) \rangle = 0, \qquad \langle \eta_i(t)\eta_i(t') \rangle = \delta(t - t') \tag{A.2}$$

where $\langle ... \rangle$ denotes the averaging operator. Equation (A.1) can be rewritten in terms of a n-dimensional Wiener process $\vec{W}$.

$$d\vec{x} = \tilde{A}\vec{x}\, dt + \tilde{B}\, d\vec{W}\,. \tag{A.3}$$

The generalized derivative of a Wiener process is Gaussian white noise $\vec{\eta}$. Common examples of Wiener processes are Brownian motion or the continuous random walk. The solution of this SDE is given by (see e.g., Gardiner

1985; Horsthemke and Lefever 1984; Kloeden and Platen 1992)

$$\vec{x}(t) = \exp(\tilde{A}t)\vec{x}(0) + \int_0^t \exp[\tilde{A}(t-t')]\tilde{B}\, d\vec{W}(t')\,. \qquad \text{(A.4)}$$

The solution requires the explicit knowledge of the matrix exponential function $\exp(\tilde{A})$. The corresponding covariance matrix is

$$\begin{aligned} \langle \vec{x}(t)\, \vec{x}^T(s)\rangle &= \exp(\tilde{A}t)\langle \vec{x}(0)\, \vec{x}^T(0)\rangle \exp(\tilde{A}s) \\ &+ \int_0^{min(t,s)} \exp[\tilde{A}(t-t')]\tilde{B}\tilde{B}^T \exp[\tilde{A}^T(s-t')]\, dt'\,. \end{aligned} \qquad \text{(A.5)}$$

The integral can be explicitly evaluated in certain special cases, as long as the matrix exponential function is known (see e.g. Braun (1993) for techniques to determine explicit expressions for matrix exponential functions). The spectra and cross-spectra can be evaluated by Fourier transforming the appropriate elements of the covariance matrix.

Using the stochastic process described by (9), the elements of the covariance matrix become:

$$\langle x_1(t)\, x_1(s)\rangle = \frac{\sigma_1^2}{2a}\exp(-a|t-s|) \qquad \text{(A.6)}$$

$$\begin{aligned} \langle x_1(t)\, x_2(s)\rangle &= \frac{\sigma_1^2 c}{2a(b-a)}\exp(-a|t-s|) \\ &- \frac{\sigma_1^2 c}{(b^2-a^2)}\exp(-at-bs+(a+b)min(t,s)) \end{aligned} \qquad \text{(A.7)}$$

$$
\begin{aligned}
\langle x_2(t)\, x_2(s)\rangle &= \frac{\sigma_1^2 c^2}{2a(b-a)^2}\exp(-a|t-s|) \\
&- \frac{\sigma_1^2 c^2}{(a+b)(b-a)^2}\exp(-at-bs+(a+b)min(t,s)) \\
&- \frac{\sigma_1^2 c^2}{(a+b)(b-a)^2}\exp(-bt-as+(a+b)min(t,s)) \\
&+ \frac{\sigma_1^2 c^2}{2b(b-a)^2}\exp(-b|t-s|) \\
&+ \frac{\sigma_2^2}{2b}\exp(-b|t-s|)\,. \qquad \text{(A.8)}
\end{aligned}
$$

Note that the covariance matrix is of course symmetric: $\langle x_1(t)\, x_2(s)\rangle = \langle x_2(t)\, x_1(s)\rangle$.

References

Bracco, A., J. H. LaCasce, and A. Provenzale, 2000: Velocity probability density functions for oceanic floats. *J. Phys. Oceanogr.*, **30**, 461–474.

Braun, M., 1993: *Differential Equations and Their Applications: An Introduction to Applied Mathematics*. Springer-Verlag, 578 pp.

DelSole, T., 2000: A fundamental limitation of Markov models. *J. Atmos. Sci.*, **57**, 2158–2168.

Ditlevsen, P. D., 1999: Observation of α-stable noise induced millenial climate changes from an ice-core record. *Geophys. Res. Lett.*, **26**, 1441–1444.

Egger, J., 2001: Master equations for climatic parameter sets. *Climate Dynamics*, **18**, 169–177.

Egger, J., and T. Jonsson, 2002: Dynamic models for icelandic meteorological data sets. *Tellus A*, **54**, 1–13.

Friedrich, R., and J. Peinke, 1997a: Description of a turbulent cascade by a Fokker-Planck equation. *Phys. Rev. Lett.*, **78**, 863–866.

Friedrich, R., and J. Peinke, 1997b: Statistical properties of a turbulent cascade. *Physica D*, **102**, 147–155.

Friedrich, R., J. Peinke, and C. Renner, 2000a: How to quantify deterministic and random influences on the statistics of the foreign exchange market. *Phys. Rev. Lett.*, **84**, 5224–5227.

Friedrich, R., S. Siegert, J. Peinke, S. Lück, M. Siefert, M. Lindemann, J. Raethjen, G. Deusch, and G. Pfister, 2000b: Extracting model equations from experimental data. *Phys. Lett. A*, **271**, 217–222.

Gardiner, C. W., 1985: *Handbook of Stochastic Methods for Physics, Chemistry and the Natural Science, Second Edition*. Springer-Verlag, 442 pp.

Gille, S. T., 1999: Evaluating Southern Ocean response to wind forcing, *Phys. Chem. Earth*, **24**, 423–428.

Gille, S. T., and S. G. Llewellyn Smith, 2000: Velocity probability density functions from altimetry. *J. Phys. Oceanogr.*, **30**, 125–136.

Gille, S. T., D. P. Stevens, R. T. Tokmakian, and K. J. Heywood, 2001: Antarctic circumpolar current response to zonally averaged winds. *J. Geophys. Res.*, **106**, 2743–2759.

Gradišek, J., S. Siegert, R. Friedrich, and I. Grabec, 2000: Analysis of time series from stochastic processes. *Phys. Rev. E*, **62**, 3146–3155.

Hasselmann, K., 1976: Stochastic climate models. Part I. Theory. *Tellus*, **28**, 473–484.

Horsthemke, W., and R. Lefever, 1984: *Noise-Induced Transitions: Theory and Applications in Physics, Chemistry, and Biology*. Springer-Verlag, 318 pp.

Hughes, C. W., M. P. Meredith, and K. J. Heywood, 2000: Wind-driven transport fluctuations through drake passage: A southern mode. *J. Phys. Oceanogr.*, **29**, 1971–1991.

Imkeller, P., and J.-S. von Storch, eds., 2001: *Stochastic Climate Models*, vol. 49 of *Progress in Probability*. Birkhäuser Verlag, 398 pp.

Kloeden, P., and E. Platen, 1992: *Numerical Solution of Stochastic Differential Equations*. Springer-Verlag, 632 pp.

Llewellyn Smith, S. G., and S. T. Gille, 1998: Probability density functions of large-turbulence in the ocean. *Phys. Rev. Lett.*, **81**, 5249–5252.

Munk, W., and E. Palmén, 1951: Note on the dynamics of the antarctic circumpolar current. *Tellus*, **3**, 53–55.

Paul, W., and J. Baschnagel, 1999: *Stochastic Processes: From Physics to Finance*. Springer-Verlag, 231 pp.

Renner, C., J. Peinke, and R. Friedrich, 2001: Experimental indications of markov properties of small-scale turbulence. *J. Fluid Mech.*, **433**, 383–409.

Rintoul, S., C. Hughes, and D. Olbers, 2001: The antarctic circumpolar current system. *Ocean Circulation and Climate*, G. Siedler, J. Church, and J. Gould, eds., Academic Press, 271–302.

Sakaguchi, H., 2001: Fluctuation dissipation relation for a Langevin model with multiplicative noise. *J. Phys. Soc. Jpn.*, **70**, 3247–3250.

Schenzle, A., and H. Brand, 1979: Multiplicative stochastic processes in statistical physics. *Phys. Rev. A*, **20**, 1628–1647.

Siegert, S., R. Friedrich, and J. Peinke, 1998: Analysis of data sets of stochastic systems. *Phys. Lett. A*, **243**, 275–280.

Stommel, H., 1957: A survey of ocean current theory. *Deep Sea Res.*, **4**, 149–184.

Succi, S., and R. Iacono, 1986: Similarity solutions of the one-dimensional Fokker-Planck equation. *Phys. Rev. A*, **33**, 4419–4422.

Sura, P., 2002: Stochastic analysis of Southern and Pacific Ocean sea surface winds. *J. Atmos. Sci.*, accepted.

Sura, P., and J. J. Barsugli, 2002: A note on estimating drift and diffusion parameters from timeseries. *Phys. Lett. A*, submitted.

von Storch, H., and F. W. Zwiers, 1999: *Statistical Analysis in Climate Research*. Cambridge University Press, 484 pp.

Wearn, R. B., and D. J. Baker, 1980: Bottom pressure measurements across the antarctic circumpolar currrent and their relation to the wind. *Deep Sea Res., Part A*, **27**, 875–888.

Weisse, R., U. Mikolajewicz, A. Sterl, and S. S. Drijfhout, 1999: Stochastically forced variability in the antarctic circumpolar current. *J. Geophys. Res.*, **104**, 11049–11064.

Table 1: Parameters of the the stochastic model (8): Wind stress and wind stress curl versus bottom pressure difference.

Parameter	Stress versus bottom pressure	Curl versus bottom pressure
a	0.095	0.214
b	0.037	0.013
c	0.041	0.018
σ_1^2	0.175	0.425
σ_2^2	0.052	0.023

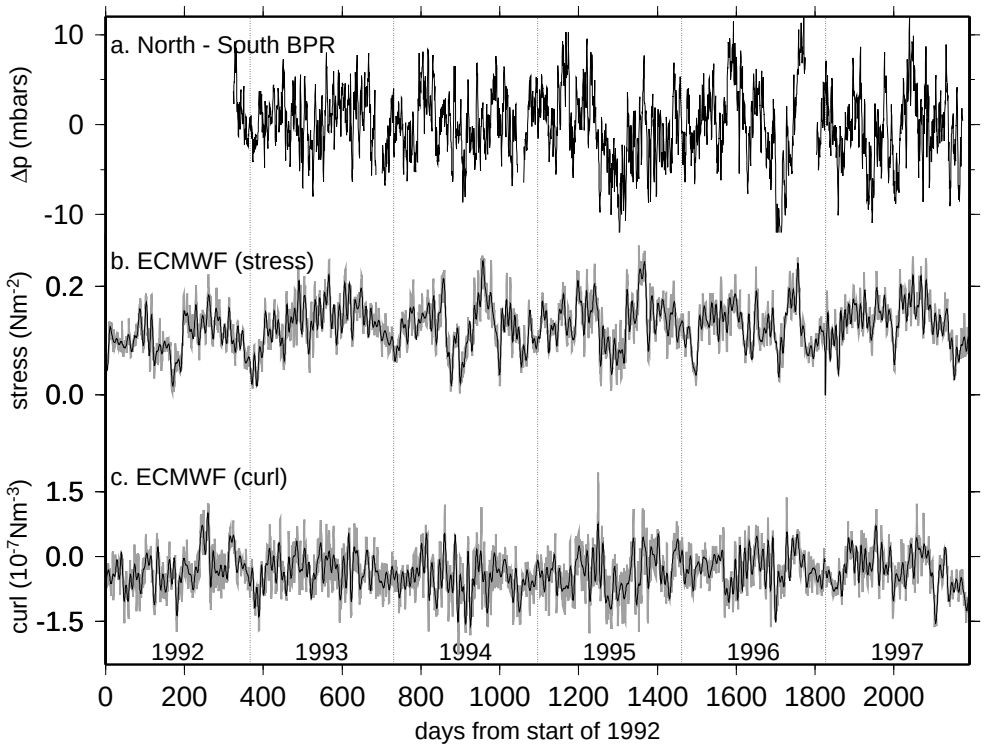

Figure 1: Time series of the data used in this study: a) Bottom pressure difference across Drake Passage, b) averaged wind stress, and c) averaged wind stress curl. For the winds, original data are shaded, and data filtered to retain only time periods longer that 10 days are solid.

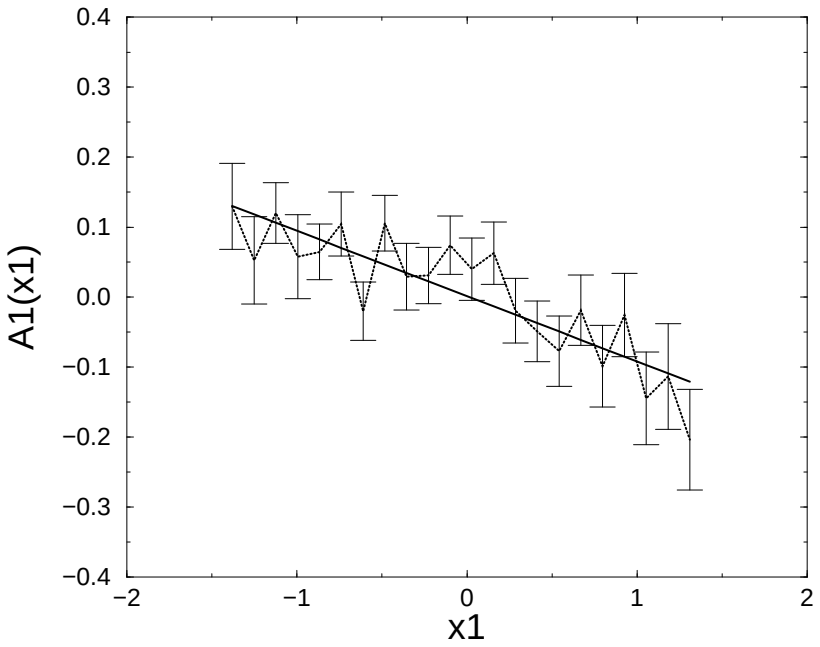

Figure 2: The estimated deterministic drift $A_1(x_1)$ for the wind stress x_1. The dashed line shows the actual estimated function. The solid line is a linear fit: $A_1(x_1) = -0.095x_1$. The error bars indicate the standard error of the mean.

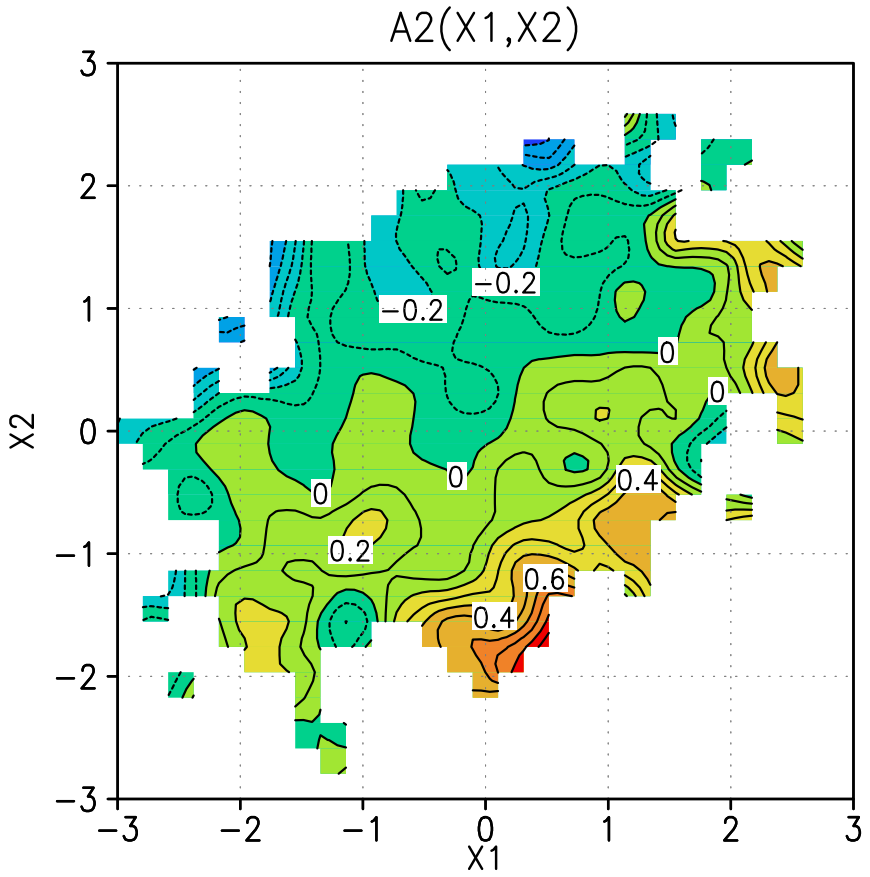

Figure 3: The estimated deterministic drift $A_2(x_1, x_2)$ for the bottom pressure difference x_2. The contour interval is 0.1, whereas the shading interval is 0.2. A two-dimensional linear fit yields: $A_2(x_1, x_2) = 0.041\, x_1 - 0.037\, x_2$.

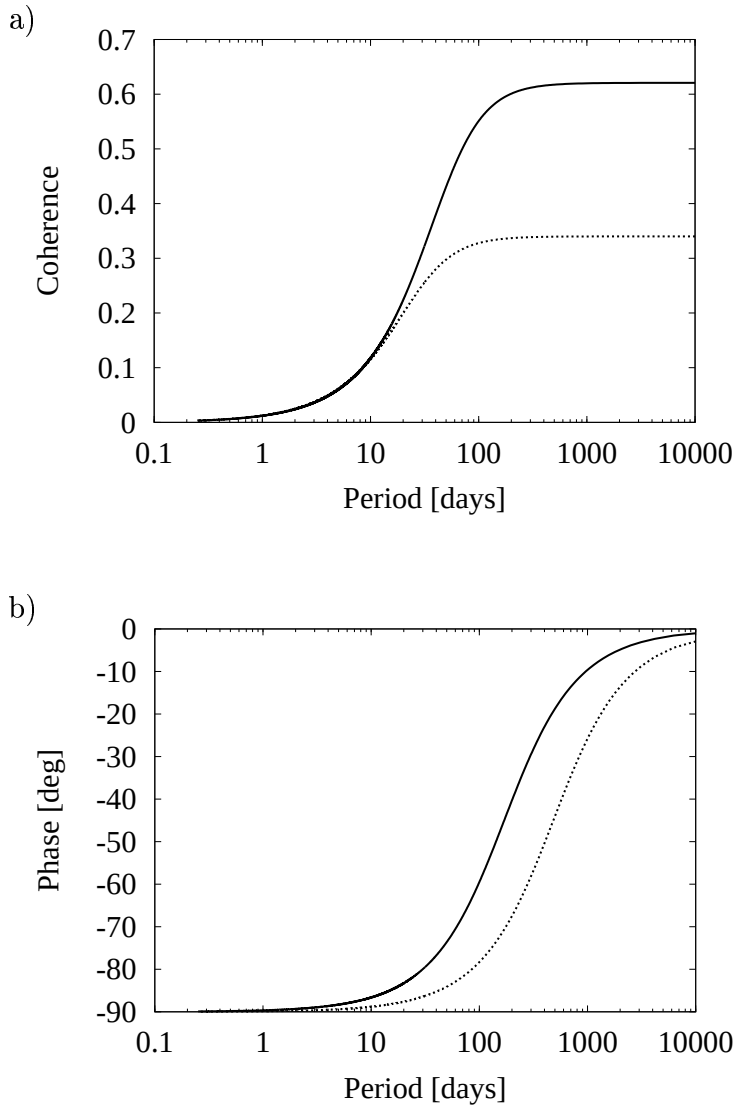

Figure 4: a) Coherence and b) phase spectra of the stochastic process (8) fitted to wind stress and bottom pressure (solid line) and wind stress curl and bottom pressure (dotted line). For clarity, the period is given in dimensional units, even if the data are nondimensional.

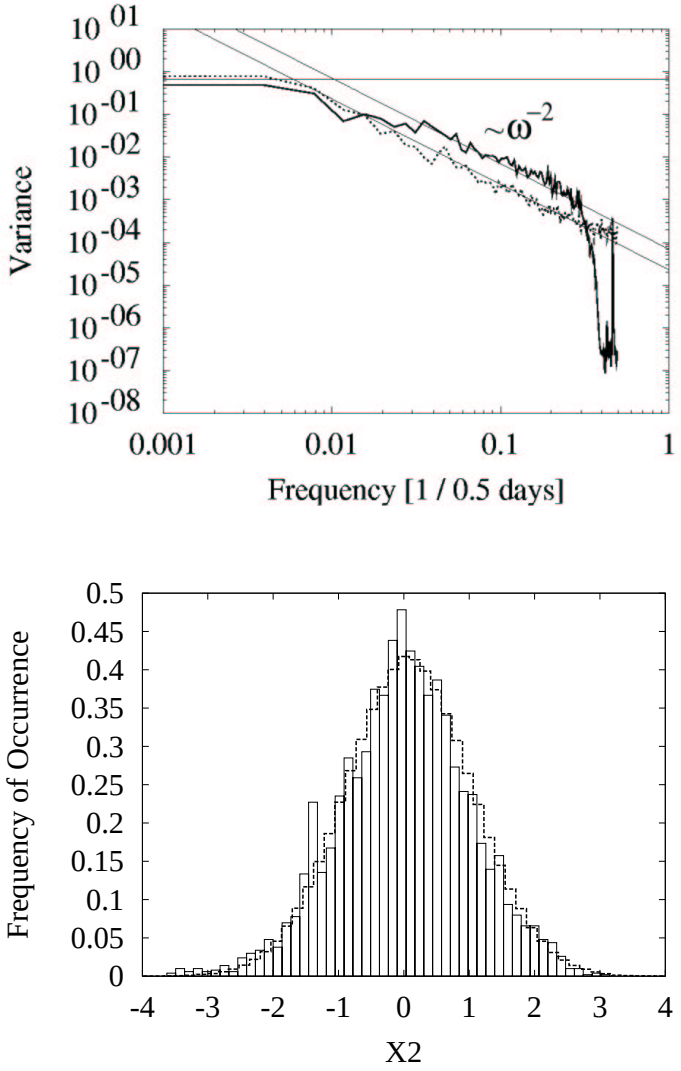

Figure 5: a) Spectra and b) histograms of the original data (solid lines) and data obtained by the SDE using the estimated parameters (dashed lines). The spectral slopes $\propto \omega^{-2}$ and $\propto \omega^{0}$ are indicated by the thin solid lines. For clarity, the frequency is given in dimensional units, even if the data are nondimensional.

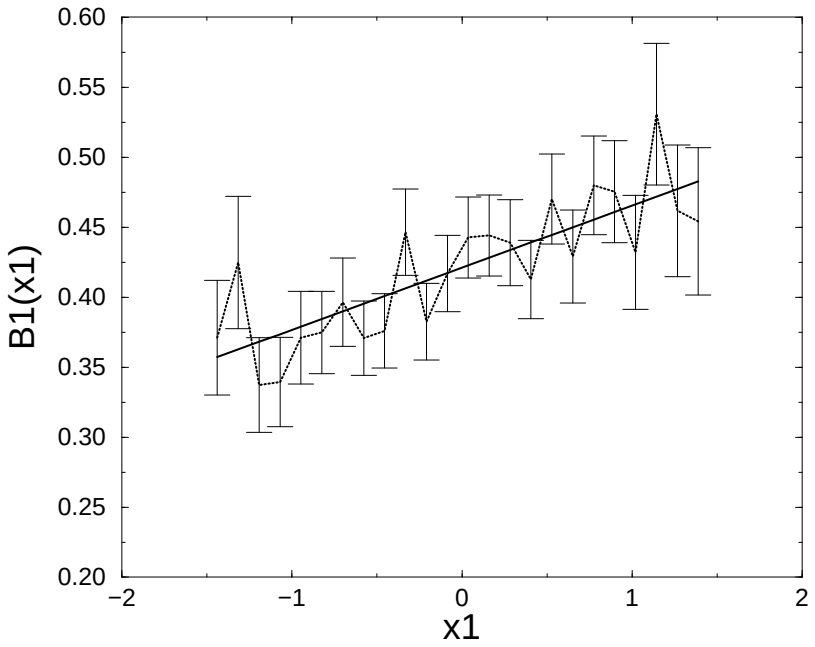

Figure 6: The estimated noise $B_1(x_1)$ for the wind stress x_1. The dashed line shows the actual estimated function. The solid line is a linear fit: $B_1(x_1) = 0.044x_1 + 0.42$. The error bars indicate the standard error of the mean.

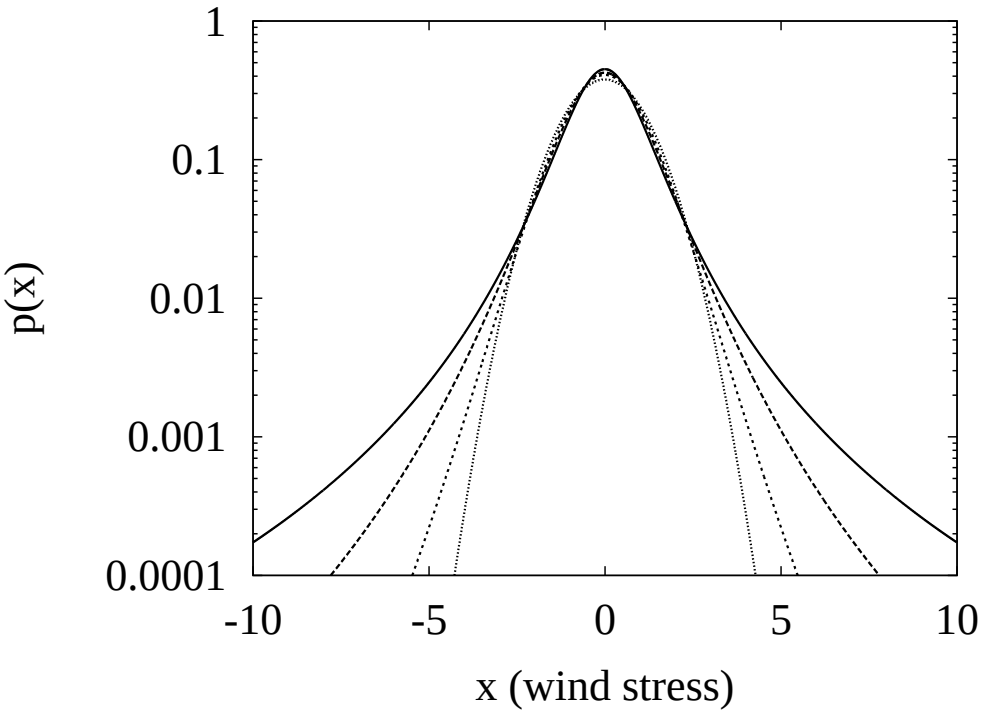

Figure 7: Stationary wind stress probability distributions $p(\tau)$ given by Eqs. (19) and (20) for $a = 1$, $D = 1$, and different strengths of the multiplicative noise: $M = 0.5$ (solid line), $M = 0.25$ (long dashed line), $M = 0.1$ (short dashed line), and $M \to 0$ (dotted line). For $M \to 0$ the distribution becomes Gaussian with the variance D/a.